ER-2 Doppler Radar (EDOP) Investigations of the Eyewall of Hurricane Bonnie During CAMEX-3

G. M. Heymsfield[1], J. Halverson[2], J. Simpson[1], L. Tian[3]and P. Bui[4]

[1]NASA Goddard Space Flight Center, Greenbelt, MD

[2]JCET, University of Maryland Baltimore County (UMBC), Baltimore, MD

[3]Universities Space Research Associates, Seabrook, MD

[4] NASA Ames Research Center, Moffut Field, CA

August, 2000

For submission to Journal of Applied Meteorology

Corresponding author address:

Gerald M. Heymsfield, NASA GSFC, Code 912, Greenbelt, MD 20771.

ABSTRACT

A persistent, mesoscale region of intense eyewall convection contained within Hurricane Bonnie on 23 August 1998 is examined from multiple observations synthesized from the NASA ER-2 and DC-8 aircraft. The intense convection occurred late in the day as Bonnie was attaining its minimum central pressure and during a stage when the inner core featured a markedly asymmetric structure. The main purpose of this paper is to describe the internal structure of a convective burst and its relationship to the warm core using a synthesis of high-resolution satellite, aircraft radar, and *in situ* data. An exceptionally vigorous eyewall tower penetrating to nearly 18 km is described. A second intense eyewall tower, adjacent to the eye, is shown to be associated with a mesoscale subsiding current of air that extends horizontally nearly 20 km into the eye interior. The subsidence occupies a substantial depth within the eye and appears to be a much larger scale feature than the convectively-induced, symmetric overturning which commonly occurs on the upper-level flanks of convective towers in other tropical environments.

1.0 Introduction

Factors leading to changes in hurricane intensity, especially at landfall, are of vital importance. Intensity forecasts have little skill and have shown only slight improvement in the past 20 years (DeMaria and Kaplan, 1999). Several factors have been identified which contribute to sudden intensification, such as warmer sea surface temperatures and dynamically forced strengthening of the upper-level outflow (Riehl, 1950). Gray (1998) has hypothesized sudden penetration of convergent wind surges near the surface, leading to unusually intense convection from inflow of high equivalent potential temperature (θ_E) air. This high energy air is carried aloft by giant cumulonimbus "hot towers" (Malkus and Riehl) leading to warming of the inner core. It is in light of these hot towers that we examine an example of intense, long-lived episodes of deep convection within the eyewall of deepening tropical cyclone Bonnie, often referred to as "convective bursts". Several case studies spanning nearly thirty years, pioneered by Gentry et al. (1970) and more recently by Holliday and Thompson (1979), Steranka et al. (1986), Zehr (1992), Lyons and Keene (1994), and Rodgers et al. (1998), point toward a relationship between the occurrence of convective bursts and sudden intensification. In this paper, we define a convective burst as a mesoscale group or succession of hot towers topped by an anomalously cold anvil cloud mass (seen in geostationary IR imagery). The anvil rapidly expands with time, remaining stationary relative to the center location for several hours. Some of the deep cumulonimbi or "hot towers", many of which may be exceptionally vigorous and overshoot their equilibrium level.

In addition, recent hurricane intensity change studies have focused on warm core anomalies observed in microwave satellite observations (Kidder et al.

1978; Velden et al. 1991). A recent study utilizing data from the Advanced Microwave Sounding Unit (AMSU) on NOAA-15 (Velden et al. 1999) confirmed that significant warming occurred through deep layers in the eyes of hurricane Georges and Bonnie during 1998. This latter work a link between the magnitude of the satellite-derived warm core and the surface pressure at the storm center assuming the storm was in hydrostatic balance . What has not been well understood however, is the details of the mechanisms producing these warm cores. This important and controversial issue has been addressed with models (Smith 1980; Zhang et al. 2000) and observations (Malkus 1958; Kuo 1959; Shapiro and Willoughby, 1982; Willoughby 1999). Many of the proposed mechanisms linking core warming with deepening of the storm invoke an important role for subsidence in the eye. In most convective burst studies, information on burst morphology and the relationship of the warm core was obtained from views obtained from passive remote sensors. In this paper, we provide detailed observations on the internal three-dimensional structure of a convective burst, including examples of vigorous hot towers and the air motions contained within them. Unique to this study is observational evidence for a broad current of strong (several meters per second) descent induced on the flank of intense convective hot towers, contained within the larger envelope of a convective burst, and penetrating deep within the warm core of the developing eye.

The NASA ER-2 and DC-8 participated with three NOAA aircraft (NOAA-42 and NOAA-43 WP-3D Orion aircraft, and the G-IVSP Gulfstream aircraft) on a comprehensive study of Hurricane Bonnie on 23 August 1998

during the Convection and Moisture Experiment-3 (CAMEX-3)[1]. CAMEX-3 focused on hurricane objectives including synoptic flow and inner core dynamics. The mission goals for 23 August were to discern eyewall structure of a moderate, nearly-stationary hurricane, and to provide improved initial conditions for track models[2]. A variety of remote sensing instruments including radars, microwave, visible to infrared range radiometers, and lidar were flown on the ER-2 and DC-8. In addition, the DC-8 carried *in situ* sensors for meteorological parameters and microphysics measurements.

The ER-2 was instrumented with the ER-2 Doppler Radar (EDOP) which is an X-band (9.6 GHz) Doppler radar with dual 3° beam width antennas fixed at nadir and 30° forward of nadir (Heymsfield et al. 1996). Data sets from EDOP will be a principle focus in this paper, corroborated by *in situ* flight level measurements and dropsondes deployed within the eye and in the environment of intense convection. In Section 2 of this paper, we present a concise description of the various observational platforms utilized throughout the study. In Section 3, the morphology of the convective burst associated with the subsidence is discussed in terms of its larger-scale, dynamic evolution as viewed from satellite. In Section 4, the fine-scale structure of hot towers and subsident region contained within the convective burst is presented from the vantage of the EDOP . These findings are summarized in Section 5 along with discussion of possible mechanisms leading to broad-scale sinking motion in the eye region and its importance in the formation of Bonnie's warm anomaly.

[1] Camex-3 web page, http://ghrc.msfc.nasa.gov/camex3.
[2] Mission Summary for flight 980823H, obtained from NOAA Hurricane Research Division (HRD).

2.0 Data and methods

2.1 EDOP processing and analysis

Details of the EDOP instrument may be found in Heymsfield et al. (1996). During the 23 August 1998 Bonnie flight, data were collected on the EDOP nadir beam with a 37.5 m gate spacing, and a pulse-repetition-frequency of 4400 Hz providing a Nyquist velocity of about 34 ms^{-1}. Processed reflectivities and Doppler velocity were obtained every 0.5 s, which corresponds to approximately 100 m of aircraft translation (aircraft ground speed ~ 200 - 220 ms^{-1}). This oversamples precipitation but is performed to maximize resolution near cloud top and to allow for better aircraft motion corrections. The reflectivity data have been calibrated to within about 1 dBZ. These reflectivities are corrected for attenuation using the surface reference approach (Iguchi and Meneghini 1994). The accuracy of this correction was slightly compromised since EDOP's nadir "surface" channel was not available and the surface return saturated the receiver in some of the lighter rain (weaker attenuation) periods. The mean Doppler velocity measurements have a standard deviation of about 0.1 ms^{-1} for typical rain situations and excluding aircraft motions which can produce significantly larger uncertainties.

Calculation of vertical air motions, w, from the EDOP-measured Doppler velocities have been described in Heymsfield et al. (1999). A number of steps are involved in going from the measured nadir-beam Doppler velocities v_D, to gridded vertical velocity fields. Aircraft motions are first removed from the v_D using flight parameters from the ER-2 inertial navigation system (INS) and the antenna tilt angles (the nadir antenna is not exactly pointed at nadir). The Doppler velocities with aircraft motion removed are vertical hydrometeor

motions (v_h) from which the vertical air motion $w = v_h + v_t$ can be obtained with a hydrometeor fallspeed (v_t) assumption based on the reflectivity. The v_h and reflectivity measurements are interpolated to two-dimensional grids with identical sampling as the nadir measurements (100 m horizontal, 37.5 m vertical) to correct for pitch variations of the aircraft. Minor filtering of the grids was performed both horizontally and vertically.

Calculation of w requires estimation of the v_t at each grid point. The v_t estimation is the most critical assumption in obtaining w since v_t depends on many factors such as particle phase, size distributions, etc. The approach is similar to that used by Marks and Houze (1987) and Black et al. (1996) which uses *reflectivity* -v_t relations relations for the snow, rain, transition (melting), and convection regions. Stratiform regions are separated vertically into three regions: rain, snow, and transition region corresponding to the melting layer. Their approach was modified slightly for EDOP observations by using a more realistic rain *reflectivity* -v_t relation derived for a gamma distribution and also a parabolic profile is assumed in the transition region instead of a linear profile (Heymsfield et al. 1999). Details of the partitioning are described in the aforementioned papers. Difficulties in fallspeed estimation occur in mixed phase regions associated with convection where strong updrafts can loft liquid water, frozen rain, and graupel several kilometers above the melting level. Fallspeeds in these regions are usually between those of snow and rain but can be larger than rain for small hail detected by EDOP in a mid-latitude squall line (Heymsfield et al. 1999). Thus, w estimates are subject to errors mainly from improper aircraft

motion removal and v_t estimation, where larger errors occur in the convective region.

2.2 In situ meteorological parameters

The DC-8 *in situ* measurements were comprised of standard flight-level measurements using the Data Acquisition and Display (DADS), plus special higher accuracy humidity and wind measuring instruments. Temperature, pressure, and humidity measurements were provided by the DADS system. Humidity measurements were measured by four separate instruments, but this study uses data only from the JPL Laser Hygrometer which is the best documented with high accuracy (May 1998). This instrument is based upon a near infrared tunable diode laser source operating near 1.37 μm. Originally designed for stratospheric measurements, its precision is 0.05 ppmv (parts per million volume) in the stratosphere, and also very good at lower altitudes. The temperature, pressure, and humidity measurements were used to calculate θ_E using the method described by Bolton (1980). The Meteorological Measurement System (MMS) on the DC-8 (Bui 1997) provided high-accuracy 5 Hz wind measurements in addition to independent temperature and pressure measurements. Accuracies of the MMS are: pressure (∓0.3 hPa), temperature (∓0.3 °C), horizontal wind vector (∓1 ms^{-1}), and vertical wind vector (<1 ms^{-1}).

3.0 Evolution of the Convective Burst: Mesoscale Structure

3.1. Satellite IR evolution.

The initial intensification of Bonnie from tropical depression to huricane status commenced late in the day on August 20, 1998. (Fig. 1). Hurricane Bonnie first developed an eye early on 22 August, with the deepening trend continuing until a surface minimum pressure of 954 hPa was reached near 0000 UTC on 24 August. During the intensification period, convective bursts were noted in both the satellite IR observations and also by the NASA aircraft pilots. An initial burst formed adjacent to the evolving eye late on 21 August. Its hot towers observed during the aircraft mission were overshooting the tropopause to at least 17 km Within 6 h of this burst, a closed eye appeared in the satellite imagery. In addition, on 22 August, the TRMM Precipitation Radar (PR) again observed an exceedingly tall hot tower or "chimney" cloud in the inner eyewall that topped 18 km. The maximum surface winds of about 52 ms^{-1} were reached and maintained after these episodes of intense convective activity and near the time of the minimum surface pressure (0000 UTC, 24 August).

The intensification of Bonnie is shown in Fig. 2 with a larger scale sequence of GOES IR satellite imagery from 1645 on 23 August (panel A) to 0215 on 24 August (panel F). The coldest IR temperatures with $T_b < 200$ K are depicted by white regions embedded in the overall cloud shield (mostly red colors), and defines the mesoscale extent of the burst. This sequence indicates a strongly asymmetric region of coldest cloud top temperatures undergoing a pronounced expansion between 1915-0015, and with the most active convection concentrated in the north and east quadrants of Bonnie. The asymmetric mesoscale burst in the inner eyewall (most evident after 23/2015) persists for about 10 h in the same location relative to the center of the vortex. Persistent formation of intense convective cells in the same quadrant of the eyewall is often

observed in tropical cyclones (Simpson, 1966; Gentry, 1970),and in the case of Bonnie, may have been caused by a convergent region established by a low-level jet identified in the NOAA-42 WP-3D aircraft flight level wind analysis (see footnote 2). Other interesting features of the temperatures are episodes of erosion of the cloud shield on the west half (forward quadrants) of Bonnie (e.g., August 23 at 1645 UTC [panel A], August 24 at 0215 UTC [panel F]etc.) presumably due to intrusion of drier air on the forward quadrants of the storm.

Focussing on the finer scale structure of this burst reveals considerable evolution in the coldest IR areas (Fig. 3). The GOES IR temperatures from the inner core region are shown in Fig. 3 for a period covering the aircraft flights (1846 to 2145 UTC). During this sequence, GOES was in a short interval mode and images were collected at approximately 7.5 min intervals. The inner core region and approximate inner eyewall location is about 100 km in diameter and is shown on the images assuming no change in diameter over the 3-hour period. The convective activity is strong during the sequence, and the coldest temperatures are east and north of the circulation center in the left rear quadrant. Several hot towers labeled Cells A, B, C, and D persist for 30 min or more with minimum temperatures 190-195 K, and are presumed to be associated with tall overshooting convection along the northeast eyewall of Bonnie. The cells develop in succession near the same genesis region before 2100 UTC, then weaken, and finally advect cyclonically and outward from the eyewall. After 2100, convective activity increased along the eastern eyewall. Of particular interest is the fact that a portion of the cirrus outflow from the vigorous cells advects over the eastern portions of the inner core which causes the eye to be obscured by a cirrostratus layer. This cirrostratus is also very significant in that

portions contain the deep subsidence in the eye as described in more detail in Section 4. It is noteworthy that in Fig. 3 the eyewall is partially open until 2145 UTC.

3.2 . Interrelation between upper-level warm anomaly, winds, IR temperatures, and low-level radar reflectivity.

The warm anomaly has long been known to be related to hurricane intensity (see, for example Malkus and Riehl, 1960; Hawkins and Riebsame, 1968). For later discussion of EDOP observations of eyewall and convective burst structure in Bonnie, two-dimensional maps of *in situ* measurements were constructed from the DC-8 flight-level data. TheDC-8 flew multiple passes across Bonnie at 11.75 km ∓0.2 km altitude over a ~2.8 h period, thereby allowing for construction of a two-dimensional map of thermodynamic parameters and winds under a quasi-steady state assumption (Fig. 4). Figures 4a-4b, and 4c-4d correspond respectively to two EDOP flight lines beginning at about 1950 and 2115 and which are described in detail later. Figure 4a shows two-dimensional maps of θ_E, Meteorological Measurement System (MMS)-derived horizontal wind, GOES IR brightness temperature at 1955 UTC enhanced for cold cloud tops, vertical motion regions exceeding $|3\ ms^{-1}|$, and DC-8 dropsondes release locations. θ_E is a conserved quantity and has been widely used for studying hurricane warm cores (Malkus and Riehl, 1960; Simpson et al., 1998).Figure4b shows a composite radar image from the NOAA-42 aircraft C-band lower fuselage radar at 1950. Figures 4c and 4d are similar to Figs. 4a and 4b except focused on the second period near 2115, and mixing ratio plotted in Fig. 4c

instead of θ_E. Evident at both times are an asymmetric eyewall with most of the heavy rain on the east side of the eye (Figs. 4b and 4d), and a complete absence of an eyewall in the northwest and southwest quadrants.

Figure 5 shows skew-T plots and height profiles of θ_E from selected four of the ten dropsonde releases from the DC-8. The locations of these dropsonde releases are shown in Figs. 4a and 4c except for the 1944 release which is 250 km east of the circulation center. The release at 1859 (a) passes along the inner edge of the south eyewall, the 2126 release (b) passes approximately down the center of the eye, the 1944 release (c) represents the environment east of the circulation, and the 2040 release (d) represents the close-in northwest hurricane environment. The GPS position measurements failed for two of the dropsondes (2126 and 1944) and thus no horizontal winds were available. Accuracies of the GPS sondes are: pressure ($\mp$0.5 hPa), temperature ($\mp$0.2 °C), and horizontal wind vector ($\mp$0.5 ms^{-1}) (Hock and Franklin 1999). The sondes did not begin recording until about 1 km below the aircraft so the θ_E profile is extended to the DC-8 level using the aircraft value. These sondes will be referred to in later discussion.

Mapping of θ_E, winds, and mixing ratio (Figs. 4a and 4c) was performed by computer contouring the irregularly spaced data points along each of the DC-8 passes across Bonnie. These passes were at nearly constant altitude and since Bonnie's motion was quite slow during 23 August, a correction for hurricane translation was not performed. This approach is acceptable for the larger scale hurricane structure but in some instances, it may not capture details of the wind and thermodynamic structure associated with the inner core region. The θ_E contours (Fig. 4a) indicate a well-defined warm core with a 368 K maximum,

implying a 10-12 K perturbation from the ~356-358 K environmental values outside of the inner core region (Fig. 5c and the further out DC-8 *in situ* θ_E show the ambient values). The inner eyewall location is evident by the ring of vertical motions denoted by "+" in Figs. 4a, and this roughly coincides with the 362 to 364 K contours in θ_E. The mixing ratio indicates drier air north of the circulation center and moister air south and southwest of the center, although the actual values are very small at the near 12 km altitude. This moisture pattern is unexpected in view of the colder IR temperatures. But it will be seen later that the DC-8 is detecting subsidence and drying ("S_1" in Fig. 5d) below a cirrus outflow layer.

The superposition of GOES IR temperatures and lower level radar reflectivity depict a highly tilted, spiral conveyer belt of moisture within the convective burst. The low-level hurricane inflow jet is located along the left rear quadrant of the circulation[3], air ascends rapidly and wraps cyclonically toward the right front quadrant in intense eyewall convection, and exits at upper levels as cold cirrus outflow of the convective burst on the rear quadrants relative to the center of the circulation. Furthermore, the DC-8 *in situ* winds are strongest winds outside of the western and southwestern eyewall, suggesting vertical transfer of momentum in this region.

4.0 Fine Scale Structure of the Convective Burst in EDOP Observations

4.1 Hot tower "C" within eye

[3] The NOAA Hurricane Research Division reported[2] an enhanced inflow jet on the East side of Bonnie.

Figure 6 presents an EDOP flight line from 1950 to 2017 which cuts across the southern edge of "Cell C" (Fig. 3D) and typifies the fine scale structure of Bonnie's inner core. The upper panel provides attenuation corrected reflectivity, whereas the lower panel shows vertical velocities calculated as described in section 2. Traces from the DC-8 flight level θ_E and w are superimposed on the panel and centered on the mean DC-8 altitude; wind barbs are plotted with the head exactly at the DC-8 altitude (flags on barbs are 25 ms^{-1}). The DC-8 time and location were within about 160 s and 1 km, respectively for most of the line. NOAA-42 flight level data taken about 1.8 h later and within 20 km of the ER-2 and DC-8 flight lines are also superimposed giving a lower level view. Similar to the radar composite (Fig. 4b), the eastern eyewall is quite active with peak reflectivities greater than 50 dBZ in the inner eyewall (x~100 km where x corresponds to distance axis) extending from the surface to about 7 km altitude, with vertical velocities exceeding 6-8 ms^{-1} (red and white colors in Figure 6These are typical magnitudes found in the updrafts of hurricane eyewalls (Black et al. 1996). The reflectivities were attenuated approximately 8 dBZ and were therefore attenuation corrected as described previously. The peak height of the eyewall updraft is approximately 16.5 km. There is also significant stratiform rain further to the east and evidence of an outer eyewall (x~40 km). The western eyewall (x~160 km) is extremely weak at upper levels, and not detected by EDOP at lower levels. EDOP is observing mainly cirrus outflow to the west, also supported by the other flight lines (not shown) and the 2044 dropsonde (Fig. 5d) with a deep subsidence beneath this cirrus layer whose base ranges up to 12 km altitude. Wind barbs from both aircraft clearly show the circulation center (x~140 km), maximum winds at the WP-3D altitude of 30 ms^{-1}, and 25 ms^{-1} at the

DC-8 altitude. The warm core is apparent in the θ_E traces with a 10 K warming at ~12 km altitude, and 14 K at ~4.5 km altitude. Two days later, on August 25, the AMSU on NOAA-15 obtained a profile of Bonnie's warm core (Kidder et al. 2000). The intensity of the storm was only slightly greater than on August 23, so that a comparison of aircraft measured temperatures to those from AMSU is useful. At the DC-8 level of 11.8 km (~39,000 ft) the temperature excess was about 8 °C in good agreement with the AMSU. The lower aircraft at 4.5 km reports a temperature excess of about 8°C also which is about twice that sensed by AMSU on August 25. However, at this level, Fig. 7 suggests that this warming may be associated with cloud and may not extend all the way across the eye, which was very wide on August 23. If the eye at low levels was smaller on August 25, the AMSU values could have been reduced by beam filling problems.

Figure 7 provides a zoomed image of Fig. 6 which emphasizes the structure of the eastern eyewall and the associated eyewall convection and strong subsidence within this portion of the eye. This eyewall has strong EDOP-derived vertical velocities, w, (denoted w_{EDOP}) exceeding 10 ms^{-1} from 3 km up to 15 km altitude and high reflectivities exceeding 50 dBZ extending from the eyewall at 7 km altitude to outside of the eyewall at the surface. The w_{EDOP} are consistent with the in situ measurements from the DC-8 and P-3 (Fig. 7, bottom) which show similar magnitudes of 8-10 ms^{-1}. The intensity of the updrafts plus high reflectivities suggests large rimed hydrometeors such as graupel or small hail falling out of the eyewall from above the freezing level at ~5.3 km altitude. The strong downdraft at 7 km altitude near the origin of this reflectivity core is

likely due to inadequately correcting for fallspeeds. That is, a snow fallspeed is assumed whereas the high reflectivities are suggestive of higher fallspeed ice particles such as dense graupel or small hail.

The pronounced mesoscale subsidence in Fig. 7 (blue colors) covers a broad 25 km wide region within Bonnie's eye (x~105-130 km) and extends from near cloud top level (15 km), down to about 6 km altitude. This subsidence region is independently confirmed by comparison of w_{EDOP} with the DC-8 *in situ* measurements (Fig. 8). Figure 8 was constructed by matching the EDOP measurement closest to the DC-8 flight level measurement, both spatially and in altitude The separation between the EDOP column and the DC-8 were greater than 4 km, the points were rejected.; points are not shown for EDOP when the reflectivity is low in the absence of scatterers. The fallspeeds with a maximum in the eyewall were calculated based on the fallspeed-reflectivity relation and adjusted for altitude as described previously.

The eyewall updraft and subsidence within the eye are independently confirmed by this figure. One main reflectivity core exists in the updraft with peak reflectivities of about 28 dBZ and maximum w_{EDOP} of about 8 ms^{-1} both from EDOP and the DC-8 MMS. The θ_E traces indicate values of 364-365 K within the updraft, transitioning across the subsidence region to 368 K within the eye. The mixing ratio is nearly constant across the updraft (0.35 gkg^{-1}), dips slightly in the transition between the updraft and downdraft (0.31 gkg^{-1}), then increases steadily to larger values in the eye.

The w curves are quite similar between the DC-8 and the EDOP. The differences can be attributed to any or all of the following: the fallspeed estimates used for correcting EDOP, errors in the w_{MMS} estimates, or displacements of the

DC-8 and EDOP measurements combined with strong gradients in w. In the downdraft region (Fig. 8, x~115 km), the DC-8 w (denoted w_{MMS}) is -3 ms^{-1} versus -6 ms^{-1} from EDOP. Fallspeeds were estimated to be 2.4 ms^{-1} associated with these peak values (Fig. 8b). To determine whether these fallspeed estimates are reasonable, the difference between the MMS and w_{EDOP} is plotted in Fig. 8b. The w_{MMS} in the updraft region (x~90-105 km)is about 4 ms^{-1} than w_{EDOP}. This difference is possibly attributed to inaccurate removal of the strong rotational wind component (Fig. 8e) from the Doppler velocities. A bias in the positioning of the antenna in roll angle is possible since strong cross-track winds directly enter into the EDOP Doppler velocities when the beam is off-nadir in roll angle; these biases were estimated but roll angle bias is more difficult to estimate since the ER-2 has small roll angles relative to EDOP's beam width. The positive difference in w_{MMS}-w_{EDOP} between x~110-115 km is likely due to improper fallspeed removal. DC-8 cloud microphysics data from this localized updraft-downdraft transition region indicated the presence of 2- 3 mm heavily rimed spherical ice particles which could be classified as graupel or possibly originating from frozen raindrops.[4] These particles would have larger fallspeeds (possibly 4-5 ms^{-1}) as compared with the snow fallspeeds assumed in calculation of w_{EDOP}, thereby producing an underestimate of w_{EDOP}.

In view of the above, there are still several important factors suggesting detrainment from the eyewall updraft into the subsidence region. First, the radial wind component shown by vectors in Fig. 8a and by the trace in Fig. 8e show strong flow across the updraft-downdraft couplet. Speed divergence between the updraft and downdraft, and speed convergence west of the

[4] Personal communication with Dr. A. Heymsfield at National Center for Atmospheric Reserarch.

downdraft suggests that the downdraft is *entraining* air out of the updraft, as first postulated by Malkus (1958). This is consistent with the MMS winds which back while passing across the updraft-to-downdraft transition (Fig. 8d, x~110 km). Furthermore, there is a pronounced reduction of wind speed (Fig. 8d, x~110 km) suggesting downward transport of smaller momentum values from high levels. Subsidence is suggested by the downward momentum transport of previously updraft air. Descent is accelerated and/or maintained by detrainment of updraft air, which supplies liquid or solid hydrometeors to vaporize and lower the density of the descending current. Other factors such as vertical pressure gradient forces also cannot be ruled out.

4.2 Structure of overshooting hot tower "D".

Figure 9 covers a covers a second vigorous overshooting hot tower (OHT) illustrated in the satellite IR temperatures (Cell D in Fig. 3a) and Fig. 4c. Figure 10 shows an enlargement of just the OHT. This tower is northwest of the circulation center and the radar cloud top extends up to 17.5 km altitude with an apparent 1.5-2 km "overshooting" region based on soundings from Puerto Rico which consistently have a sharp tropopause at 15.5 km. Similar to the previous flight line, the eyewall of the rear quadrants of the circulation center is dominated by strong convection with reflectivities exceeding 50 dBZ at low levels, whereas the eyewall structure southwest of the circulation center is weak in this respect. Furthermore, the cloud top height is below 15 km on the west side of the storm compared with the higher tops in the more convective region. The winds at the DC-8 altitude are strongest (25 ms^{-1}) in the western eyewall. At

the lower WP-3D altitudes, peak winds are about 40 ms^{-1}. A strong warm core 8-10 K warmer than the enviroment is apparent (lower panel n Fig. 9) at the DC-8 altitude, and a ~6K warm core at WP-3D altitudes except within the eyewall where θ_E is 368K. A dropsonde was released at 2126 in the eye (Fig. 5b and located in Fig 9) and indicates a deep warm core with θ_E ~366K at 12 km altitude extending down to θ_E ~360K at 5 km altitude. This is corroborated by θ_E from the WP-3D (Fig. 9) which is also approximately 360K near 5 km altitude. Three pronounced subsidence layers labeled S1-S3 are also evident in Fig. 5b.

The vertical motion structure in the hot tower D (Fig. 10) is somewhat complex with some residual updrafts at higher altitudes, but with a dominance of downward motions between 5 to 10 km altitude. Similar to Fig. 8, Fig. 11 shows a comparison of the EDOP-derived vertical velocity and the DC-8 *in situ* measurements. Reflectivities aloft are lower than the previous flight line (Fig. 7), with mainly one high reflectivity core of 20 dBZ at x~100 km. The w_{EDOP} have an updraft peak of 4 ms^{-1} at x~90 km, and downdraft peak of -6 ms^{-1} at x~100 km. The w_{MMS} are stronger in the updraft and indicate near-zero vertical velocities near x~100 km. It is surmised that these differences are due entirely to inappropriate fallspeeds with peak values of less than 2 ms^{-1} used for correcting the EDOP hydrometeor motions. The w_{MMS}-w_{EDOP} curve (Fig. 11b) suggests the fallspeed is underestimated by about 5 ms^{-1} near x~100 km where reflectivity peaks at 20 dBZ. It is further suggested that this hot tower, having an overshoot of 1.5-2 km, is entering a dissipating stage with weakening updrafts and with large rimed hydrometeors lofted to high altitudes above the DC-8 level, now falling to lower levels An overshoot of this amount theoretically would give a

peak updraft speed of 30 ms^{-1}, which is of sufficient magnitude to sustain production of large rimed ice particles.[5] Cell D cloud top is about 1 km higher than the eyewall convection Cell C's (Fig. 7), and would therefore support ice hydrometeors with larger fallspeeds.

5. Discussion

Figure 12 shows a conceptual summary of the deduced relation between the convective burst, hot towers, and warm core in Hurricane Bonnie. The observations of hot towers presented indicate a surprisingly large magnitude (3-5 ms^{-1}) downdrafts , and deep penetration of a subsiding air current into the eye of Hurricane Bonnie. The mechanism for the subsidence along the inner edge of the eyewall are hinted at by mainly circumstantial evidence but taken together provide a coherent picture. There is indirect evidence for entrainment of drier stratospheric air at the tropopause into the subsiding current within the overshooting convective tower. The subsiding air originates near the tropopause height (15 km altitude near x~108 km in Fig. 7) and is adjacent to the convective tower updraft. A reflectivity notch is noted in the top of this hot tower near the origin of the subsidence(arrow in Fig. 7), and the reflectivity values are diminished within the upper 2-3 km of the hot tower (dashed line in Fig. 7). Finally, the strongly curved, deflected reflectivity features in Fig. 7 all consistently point in direction from the updraft to the subsidence region, suggesting that the downdraft is strong enough to entrain air from the updraft, as found in less spectacular tropical clouds by Malkus (1955). These features are

[5] Based on the laboratory work of Malkus (1960) which determined that a vertical velocity of 20 ms^{-1} is needed for every 1 km of overshoot into the stratospheric air.

consistent with the discussion of winds earlier. The decrease in wind speed within the subsiding air current fit with the wind direction changes and convergent-divergent region described previously in Section 4.1 and Fig. 8. The above points together suggest that compensating subsidence of dry stratospheric air is initiated by stratospheric overshoot of the tallest hot towers. The subsidence is then sustained by entrainment into the eye of moist cloudy air from the updraft. Sublimation of the ice hydrometeors then cools the descending air and maintains the subsidence. Evidence presented by Malkus (1958) and Simpson et al. (1998) strongly suggests that dry adiabatic descent contributes to further eye warming after the hydrometeors have been fully vaporized. In addition, detrainment of latent heat of condensation (which commonly peaks in the 3-5 km layer of convective regions) may also contribute to warming inside the eye.

There is no obvious explanation why the second overshooting hot tower sampled (Fig. 10) did not show subsidence within the eye at the time observed, but instead produced localized downdrafts *within* the cell at upper levels. This suggests that if subsidence related to deep convection does indeed play a role in eye warming, it is likely to be sporadic in nature. Quite possibly not all vigorous overshooting hot towers will produce eye interior subsidence.

6. Conclusions

This paper has documented the fine scale internal structure of a convective burst episode within Hurricane Bonnie during intensification, and the relation of this burst to the warm core, using a synthesis of high-resolution data sets including GOES, EDOP aircraft radar, and *in situ* data. The multi-aircraft

flight lines over Bonnie have provided unique measurements of the vertical precipitation and thermodynamic structure at higher altitudes than previously attained. Two hot towers within the convective burst were presented which differed in several respects, possibly due to the evolution of the hot towers and their relatively short lifetimes (less than 0.5 h). A key finding is the observation of a broad current of subsiding air within the eye during one of the hot tower flight lines. The second intense hot tower with cloud tops of 17.5 km was in a dissipating state and contained mainly downdrafts *within* the tower rather than in the eye. If the warming in the eye is the result of subsidence, then this subsidence is sporadic and episodic rather than organized weaker subsidence over the entire eye. Evidence has been provided for the causes of the subsidence associated with the hot towers, but evidence is circumstantial. This subsidence appears to result from a combination of air detraining from the eyewall updraft, and stratospheric air subsiding along the inner edge of the eyewall updraft, as postulated by Malkus (1958). She was intrigued by early radar evidence (Kessler, 1957) showing the descent of eyewall cloud matter. This descent was shown to be essential by calculations from radiosonde eye and environment observations in a moderate and an intense tropical cyclone. The Bonnie data sets analyzed here have provided a unique first look at the structure of hot towers and their relationship to the warm core. This evidence is the first mesoscale data set supporting the "hot tower" hypothesis, but there still remain many unanswered questions. The frequency and distributions of hot towers and any associated subsidence regions are unknown. The relative contributions of the various subsidence producing mechanisms also needs to be addressed. Further analysis

of the current data sets and planned future experiments such as CAMEX-4 should supply crucial evidence addressing these questions.

Acknowledgements

The CAMEX-3 analysis in this paper was supported by Dr. Ramesh Kakar at NASA Headquarters with Tropical Rain Measuring Mission funds and NASA-sponsored U.S. Weather Research Program efforts. There are a number of key people in field campaign operations that deserve special credit. Excellent coordination of the aircraft flights in Hurricane Bonnie were only possible through efforts of Dr. Ed Zipser, Ms. Robbie Hood and NOAA Hurricane Research Division (Dr. Frank Marks and colleagues). Dr. Robert Simpson provided valuable suggestions on the manuscript. Dr. Bart Geerts was extremely helpful in the data collection and initial analysis of Bonnie. Dr. Steve Bidwell and Mr. Ed Zenker are greatly appreciated for the superb engineering effort on the EDOP instrument. NOAA HRD (Dr. Frank Marks, Dr. Bob Black, and Mr. Paul Willis) provided P-3 flight level data and DC-8 microphysics information used in this analysis. Other data sets were obtained through the Marshall Space Flight Center CAMEX-3 archive. Many others answered the numerous questions that arose due to the diverse nature of the data sets used in this paper.

References

Black, R.A., and J. Hallett, 1986: Observation of the distribution of ice in hurricanes. *J. Atmos. Sci.*, **43**, 802-822.

Black, M.L. , R.W. Burpee and F.D. Marks, Jr, 1996: Vertical motion characteristics of tropical cyclones determined with airborne Doppler radial velocities. *J. Atmos. Sci.*, **53**, 1887-1909.

Bolton, D., 1980: The computation of equivalent potential temperature, *Mon. Wea. Rev.*, **108**, 1046-1053.

Bui, T. P., 1997: DC-8 Meteorological Measurement System. SONEX Workshop, NASA Ames Research Center. [Available from NASA Ames Research Center, M.S. 245-5, Moffett Field, CA 94035-1000]

Chen, S.S. and W. Frank, 1993: A Numerical study of the genesis of extra-tropical convective mesovortices. J. Atmos. Sci, 50, 2401-2426.

Dodge, P., R.W. Burbee, and F.D. Marks, Jr.,1999: The kinematic structure of a hurricane with sea level pressure less than 900 mb. *Mon. Wea. Rev.*, 127, 987-1004.

Dunnavan, G. M., E. J. McKinley, P. A. Harr, E. A. Ritchie, M. A. Boothe, M. Lander and R.L. Elsberry, 1992: Tropical Cyclone Motion (TCM-92): Mini-field experiment summary. Naval Postgraduate Report No NPS-MR-93-001.</italic> 98 pp.

Elsberry, R. L., G. M. Dunnavan and E. J. McKinley, 1992: Operations Plan for the Tropical Cyclone Motion (TCM-92) min-field experiment. Tec. Rep. NP-MR-92-002, Naval Postgraduate School, Monterey, CA., 45pp.

Elsberry, R.L., B.C. Deihl, J.C-L. Chan, P.A. Harr, G.J. Holland, M. Lander, T. Neta, and D. Thom, 1991: ONR tropical cyclone motion initiative: Field

experiment summary. Tech. Rep. NPS-MR-91-001, Naval Postgraduate School, Monterey, CA 93943-5000, 106 pp.

Emanuel, K.A., 1986: An air-sea interaction theory for tropical cyclones. Part 1: Steady-state maintenance. *J. Atmos. Sci.*, **43**, 585-604.

Hock, T. F., and J. L. Franklin, 1999: The NCAR GPS dropwindsonde. *Bull. Amer. Meteor. Soc.*, **80**, 407-420.

Fritsch, J. M., J. D. Murphy and J.S. Kain, 1994: Warm core vortex amplification over land. *J. Atmos Sci.*, **51**, 1780-1807.

Gentry, R.C., T.T. Fujita and R.C. Sheets, 1970: Aircraft, spacecraft, satellite and radar observations of Hurricane Gladys, 1968. *J. Appl. Meteor.*, **9**, 837-850.

Geerts, B., G. M. Heymsfield, L. Tian, J. B. Halverson, A. Guillory, and M. I. Mejia, 2000: Hurricane Georges's landfall in the Dominican Republic: Detailed airborne Doppler radar imagery. *Bull. Amer. Meteor. Soc.*, **81**, 999-1018.

Halverson, J.B., H. Pierce, J. Simpson, C. Morales, and E. Rodgers, 1999: First TRMM satellite observations of a deep convective burst in supertyphoon Paka (1997). Preprints, 23rd Conference on Hurricanes and Tropical Meteorology, Dallas, Texas, Amer. Meteor. Soc., 997-1000.

Hawkins, H.F. and D.T. Riebsame, 1968: Hurricane Hilda, 1964 II. Structure and budgets of the hurricane on October 1, 1964. *Mon. Wea. Rev.*, **96**, 617-636.

Heymsfield, G. M., S. Bidwell, I. J. Caylor, S. Ameen, S. Nicholson, W. Boncyk, L. Miller, D. Vandemark, P. E. Racette, and L. R. Dod, 1996a: The EDOP radar system on the high altitude NASA ER-2 aircraft. *J. Atmos. Oceanic Tech.*, **13**, 795-809.

_____, I. J. Caylor, J. M. Shepherd, W. S. Olson, S. W. Bidwell, W. C. Bonçyk, and S. Ameen, 1996b: Structure of Florida thunderstorms using high-altitude aircraft radiometer and radar observations. *J. Appl. Meteor.*, **10**, 1736-1762.

_____, J. B. Halverson, and I.J. Caylor, 1999: A wintertime gulf coast squall line observed by EDOP airborne Doppler radar. *Mon. Wea. Rev.*, **127**, 2928-2949.

Holliday, C.R. and A.H. Thompson, 1979: Climatological characteristics of rapidly intensifying typhoons. *Mon. Wea. Rev.*, **107**, 1022-1034.

Houze, R.A., Jr. 1993: *Cloud dynamics*. Academic Press, 573 pp.

Iguchi, T., and R. Meneghini, 1994: Intercomparison of single frequency methods for retrieving a vertical rain profile from airborne or spaceborne radar data. J. *Atmos. Oceanic Technol.*, **11**, 1507-1516.

Jorgensen, D.P., E.J. Zipser and M.A. LeMone, 1985: Vertical motions in intense hurricanes. *J. Atmos. Sci.*, **42**, 839-856.

Kessler, E., 1957: Eye region of Hurricane Edna, 1954. *J. Meteor.*, **15**, 264-270.

Kidder, S.Q., W.M. Gray, and T.H. VonderHaar, 1978: Estimating tropical cyclone pressure and outer winds from satellite microwave data. *Mon. Wea. Rev.*, **106**, 1458-1464.

Kidder, S. Q., M. D. Goldberg, R. M. Zehr, M. DeMaria, J. F. W. Purdom, C. S. Veldon, N.C. Grody, and S. J. Kusselson, 2000: Satellite analysis of tropical cyclones using the Advanced Microwave Sounding Unit (AMSU). *Bull. Amer. Met. Soc.*, **81**, 1241-1259.

Lyons, W.A. and C.S. Keen, 1994: Observations of lightning in convective supercells within tropical storms and hurricanes. *Mon. Wea. Rev.*, **122**, 1897-1916.

Malkus, J., 1955: On the formation and structure of downdrafts in cumulus clouds. *J. Meteor.*, **12** (4), 350-357.

Malkus, J. S., 1958: On the structure and maintenance of the mature hurricane eye. *J. Meteor.*, , **15**, 337-349.

Malkus, J. S. and H. Riehl, 1960: On the dynamics and energy transformations in steady state hurricanes, *Tellus*, **12**, 1-20

Marks, F. D., and R.A. Houze, Jr, 1987: Inner core structure of Hurricane Alicia from airborne Doppler radar observations, *J. Atmos. Sci.*, **44**, 1296-1317.

May, R. D., 1998: Open-path, near-infrared tunable diode laser spectrometer for atmospheric measurements of H_20. *J. Geophys. Res.*, **103**, 19,161-19,172.

McBride, J.L., 1996: Tropical Cyclone Formation. Chapter 3, Global perspectives on tropical cyclones, World Meteorological Organization Technical document WMO/TD-No. 693. R.L. Elsberry, editor, 63-105.

McBride, J.L. and R. Zehr, 1981: Observational analysis of tropical cyclone formation. Part 2: Comparison of non-developing versus developing systems. *J. Atmos. Sci.*, 38, 1132-1151.

Riehl, H. and J. S. Malkus, 1961: Some aspects of hurricane Daisy, 1958. *Tellus*, **13**, 181-213.

Riehl, H., 1954: Tropical Meteorology McGraw-Hill, New York, 392 pp.

Rodgers, E.B., W. S. Olson, V. M. Karyampudi and H.F. Pierce, 1998: Satellite-derived latent heating distribution and environmental influences in Hurricane Opal (1995). *Mon. Wea. Rev.*, **126**, 1229-1247.

Simpson, R.H. and J. Simpson, 1966: *Why experiment on tropical hurricanes? Transactions New York Academy of Sciences*, **28** (8), 1045-1062.

Simpson, J., J.B. Halverson, B. S. Ferrier, W. A. Petersen, R.H. Simpson, R. Blakeslee, and S. L. Durden, 1998: On the role of "hot towers" in tropical cyclone formation, *Meteorology and Atmos. Physics*, **67**, 15-35.

Steranka, J., E.B. Rodgers and R. C. Gentry, 1986: The relationship between satellite measured convective bursts and tropical cyclone intensification. *Mon. Wea. Rev.*, **114**, 1539-1546.

Velden, C. S., B.M. Goodman, and R.T. Merrill, 1991: Western North Pacific tropical cyclone intensity estimation from NOAA polar-orbiting satellite microwave data. *Mon. Wea. Rev.*, **119**, 159-168.

Veldon, C. S., and K.F. Brueske, 1999: Tropical cyclone warm cores as observed from the NOAA polar orbiting satellite's new AMSU. *23rd Conf. on Hurricanes and Trop. Meteor.*, Dallas, TX, 182-184.

Willoughby, H.E., J. A. Clos, and M.G. Shoreibah, 1982: Concentric eye walls, secondary wind maxima, and the evolution of a hurricane vortex, *J. Atmos. Sci.*, **39**, 395-411.

Willoughby, H. E., 1998: Tropical cyclone eye thermodynamics. *Mon. Wea. Rev.*, **126**, 3053-3067.

Zehr, R.M., 1992: Tropical cyclogenesis in the western North Pacific. NOAA Tech. Rep., NESDIS 61, Washington, D.C., 181 pp.

Zhang, D.-L., Y. Liu, M. K. Yau, 2000: A multiscale numerical study of Hurricane Andrew (1992). Part III: Dynamically-induced vertical motion. In press, *Mon. Wea. Review.*

Figure Captions

Figure 1. Time history of Hurricane Bonnie.

Figure 2. Sequence of GOES infrared (IR) images from Hurricane Bonnie covering late on 23 August 1998 to early 24 August 1998. Color enhancement of the images highlight the cold cloud tops associated with Bonnie. Grid lines are in 1° intervals.

Figure 3. Sequence of zoomed IR images covering period of ER-2 flights. The color table highlights the cold over shooting cloud tops and the cirrus outflow from them. The dashed circular region of about 70 km in diameter provides the approximate eyewall location. Cells are labeled A-D.

Figure 4. Flight level analysis at approximately 11.8 km altitude derived from DC-8 *in situ* measurements during the period 1850-2136. Panel (a) shows θ_E, wind barbs (flag on wind barb is 25 ms^{-1}), vertical motions exceeding | 3 ms^{-1} | denoted with "+" and "-", respectively, 1955 GOES IR temperatures less than 210 K, and dropsonde locations. Panel (b) shows the NOAA-42 WP-3D lower fuselage composite radar echo at about 2100 and the ER-2 flight track near this time. Panel (c) shows mixing ratio instead of θ_E, and the 2115 GOES IR temperatures, and Panel (d) provides the composite radar image at about 2100. See text for details.

Figure 5. Dropsonde releases in Hurricane Bonnie on 23 August 1998 at: a) 1859 in edge of south eyewall; b) 2126 in eye center; c) 1944 environment ~250 km east of the circulation center; and d) 2040 in northwest close-in environment. The location of the corresponding drop points are shown in Fig. 4. Left panel shows skew-T plot. The right panel shows θ_E profile, where the "*" indicates the DC-8 value, and the dashed portion of the curve is extrapolated between the top dropsonde level and the "*"; S_x where x=0, 1, 2 indicate subsidence layers. Flags on wind barbs are 25 ms^{-1}.

Figure 6. EDOP reflectivity and vertical velocities, w, during 1950-2010 flight line. Traces show w (blue) and θ_E (white) derived from the DC-8 flight level data. Labels are shown for: outer eyewall (O), inner eyewall (I), warm core (W), circulation center (C), freezing level (FL), and radius of maximum wind (RMW). Reflectivities (w) exceeding 50 dBZ (8 ms^{-1}) are white, and w less than -8 ms^{-1} are black. Flags on wind barbs are 25 ms^{-1}. See text for details.

Figure 7. Zoom of Fig. 6 indicating eyewall subsidence. The dashed line in the reflectivity plot shows an intruding region of low reflectivity at cloud top. Arrows in this indicate suggested detrainment of mass from eyewall updraft. "S" indicates the subsidence region within the eye. Flags on wind barbs are 25 ms^{-1}. See text for details.

Figure 8. Comparison of DC-8 flight line during 1950-2017 flight line. Shown are: a) EDOP-derived w (w_{EDOP}) and DC- flight-level w (w_{MMS}), b) reflectivity,

reflectivity-derived fallspeed, and the difference w_{EDOP} - w_{MMS}, c) DC-8 flight-level θ_E and mixing ratio, and d) DC-8 flight-level wind speed and direction, and e) DC-8 flight-level rotational and radial wind. See text for details.

Figure 9. Similar to Fig. 6 except for 2115-2134 flight line. Locations of dropsonde start time and fall trajectory are shown; numbers next to trajectory indicate distance in kilometers into (>0) or out of (<0) the plane of the cross section.

Figure 10. Zoom of convective burst in 2115-2141 ER-2 flight line similar to Figure 7.

Figure 11. Similar to Fig. 9 except for 2115-2141 flight line.

Figure 12. Conceptual summary of Bonnie structure on 23 August 1998 derived from aircraft and satellite observations.

Hurricane Bonnie Evolution (Best Track)

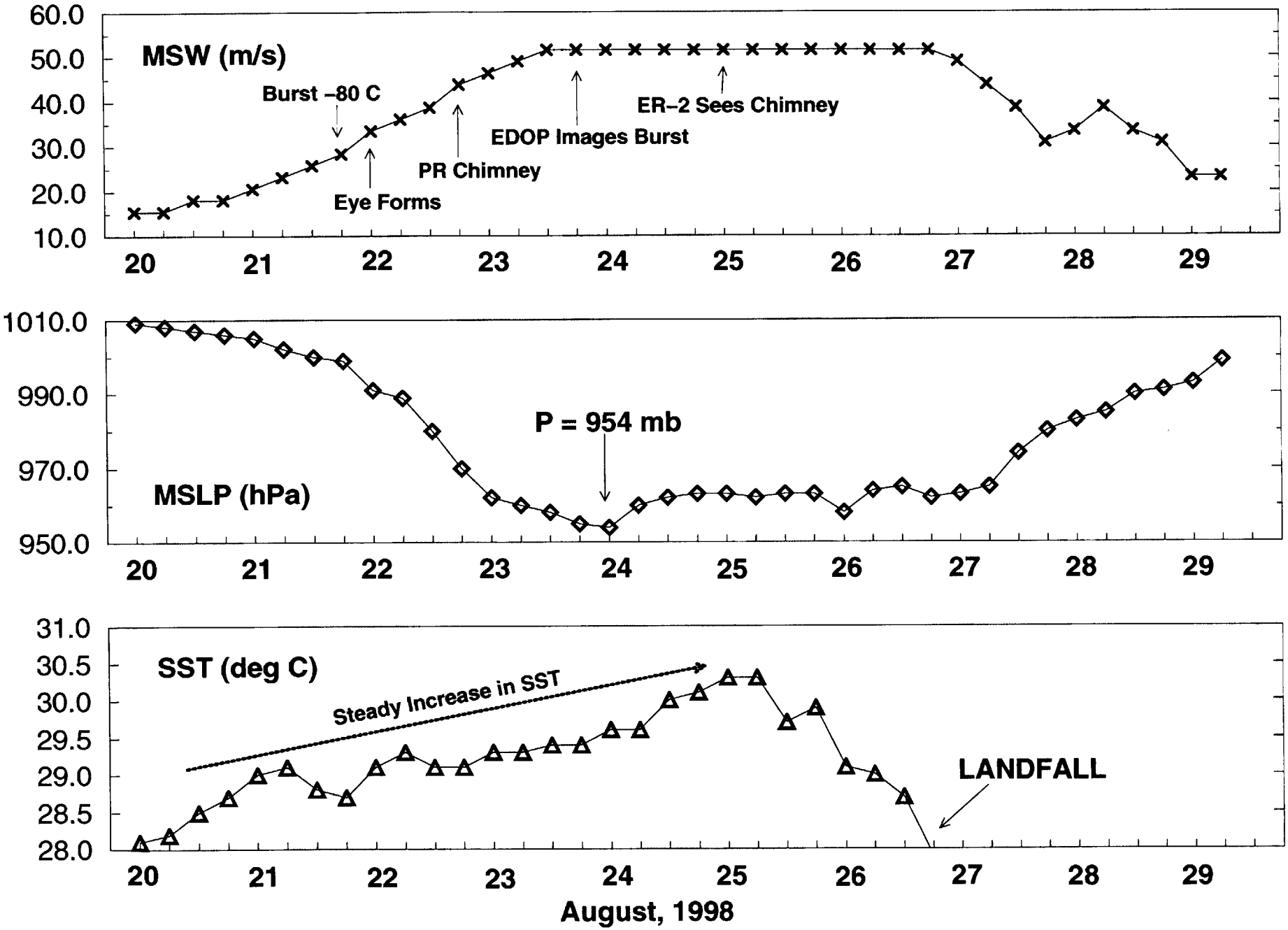

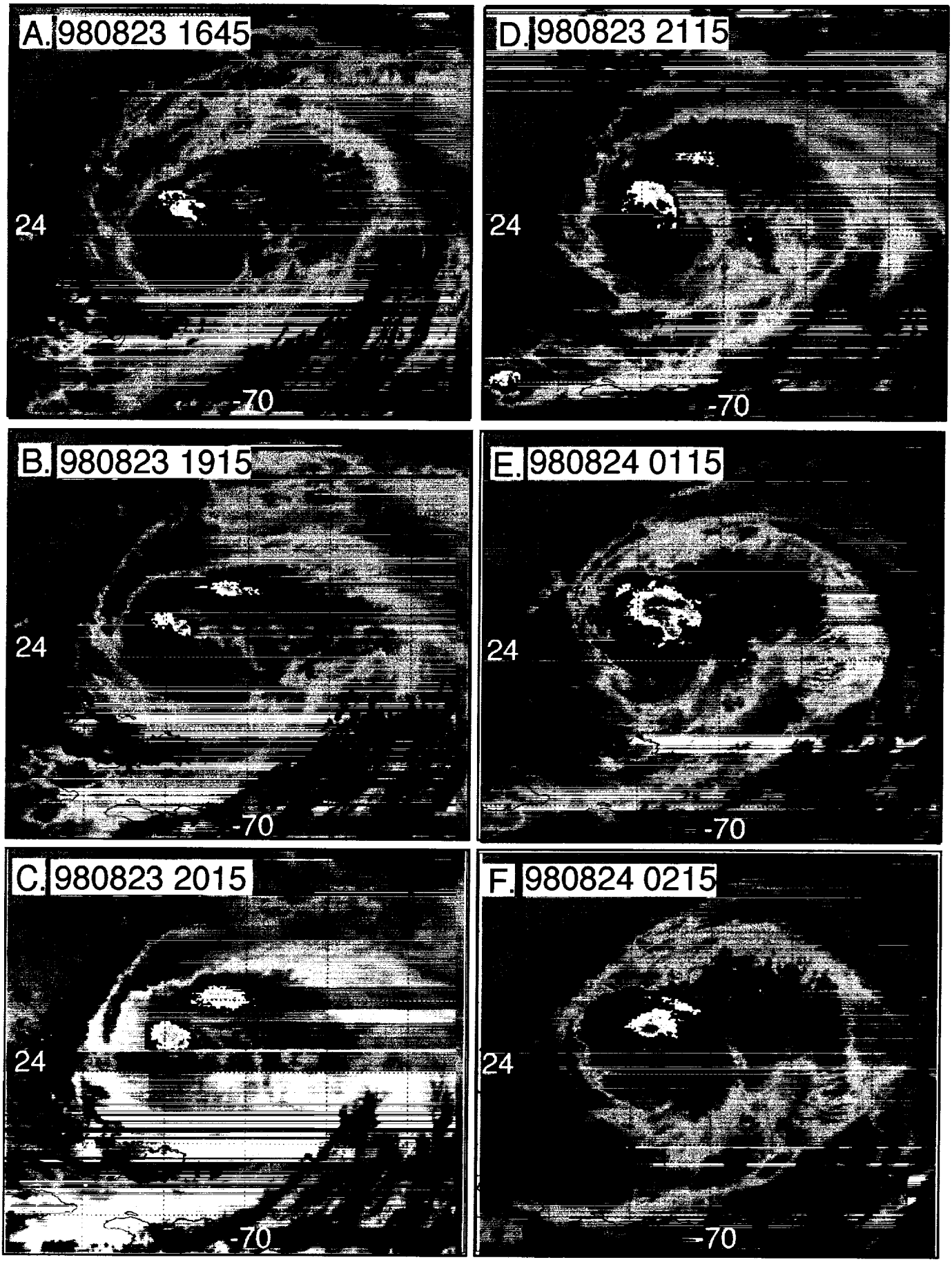
A. 980823 1645
24
-70
D. 980823 2115
24
-70
B. 980823 1915
24
-70
E. 980824 0115
24
-70
C. 980823 2015
24
-70
F. 980824 0215
24
-70
190 210 230 250 270 290 310 330
TEMPERATURE (K)

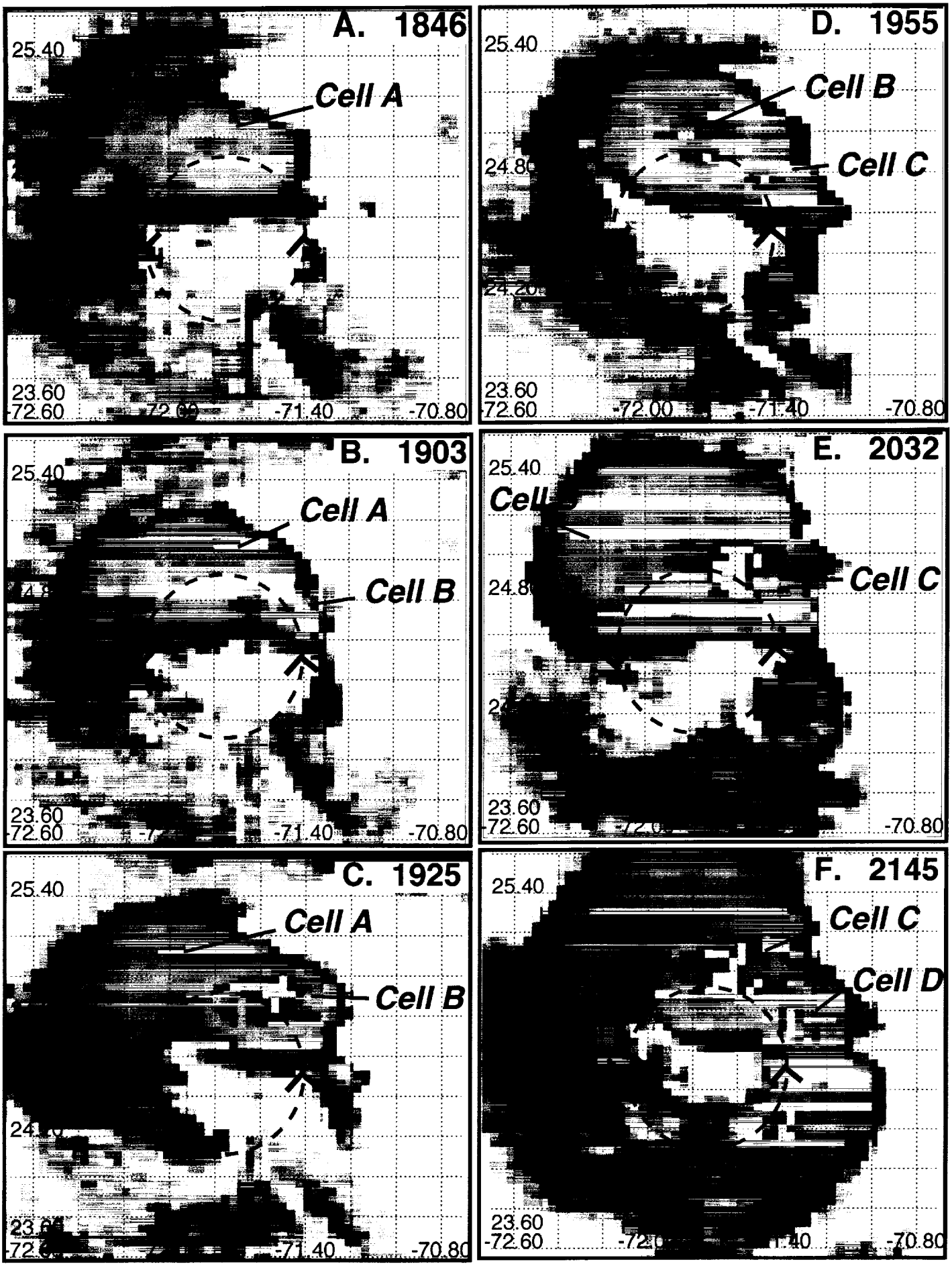
A. 1846
Cell A
25.40
23.60
-72.60
-71.40
-70.80
D. 1955
Cell B
Cell C
25.40
23.60
-72.60
-72.00
-71.40
-70.80
B. 1903
Cell A
Cell B
25.40
23.60
-71.40
-70.80
E. 2032
Cell C
25.40
23.60
-72.60
-70.80
C. 1925
Cell A
Cell B
25.40
-71.40
-70.80
F. 2145
Cell C
Cell D
25.40
23.60
-72.60
-70.80
190
195
200
205
210
TEMPERATURE (K)

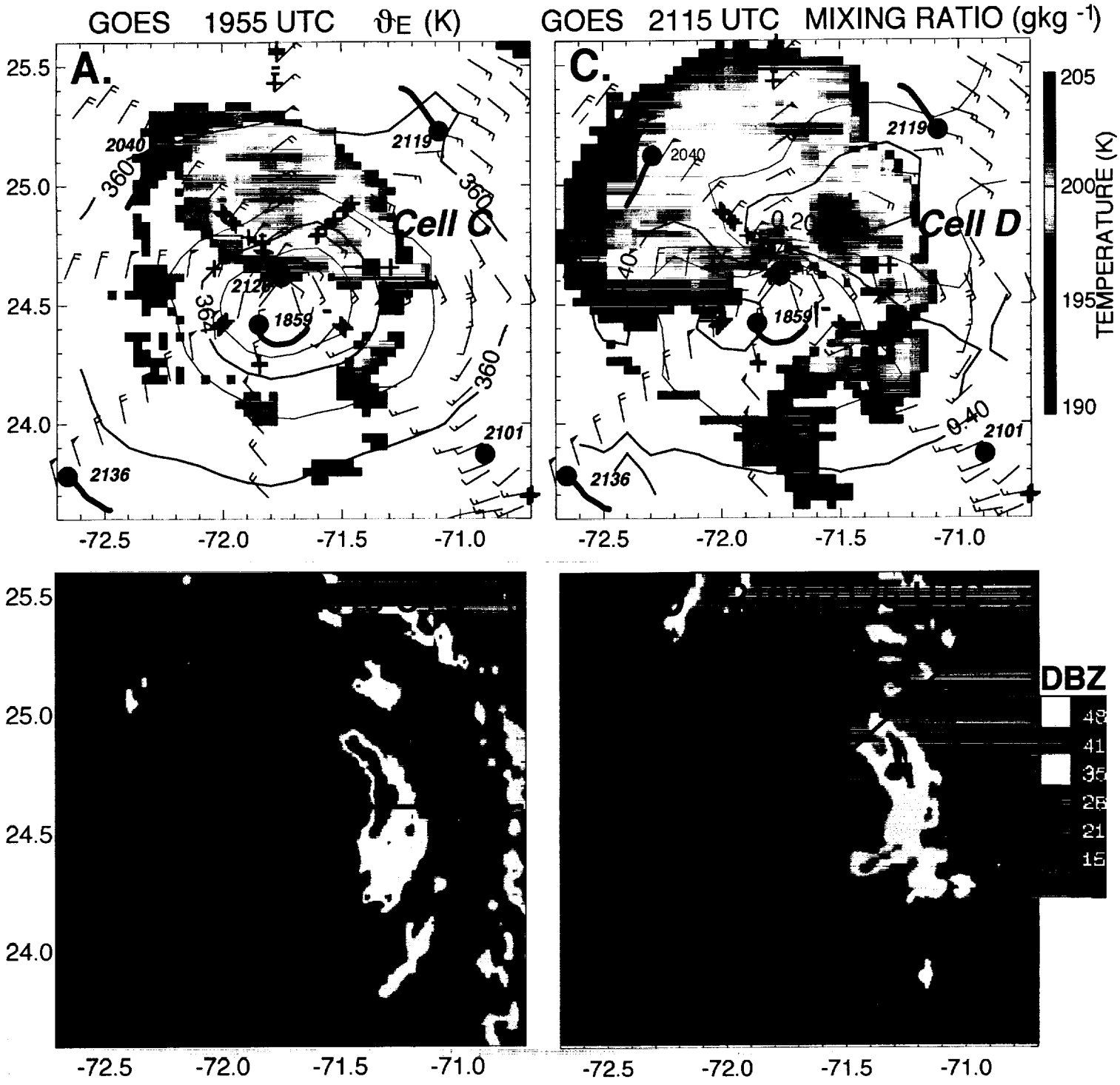
GOES 1955 UTC ϑE (K)
GOES 2115 UTC MIXING RATIO (gkg -1)
A.
C.
Cell C
Cell D
2040
2119
2120
1859
2101
2136
360
340
320
300
280
260
240
220
200
180
160
140
120
100
80
60
40
20
0
TEMPERATURE (K)
205
200
195
190
DBZ
48
41
35
28
21
15
25.5
25.0
24.5
24.0
-72.5
-72.0
-71.5
-71.0

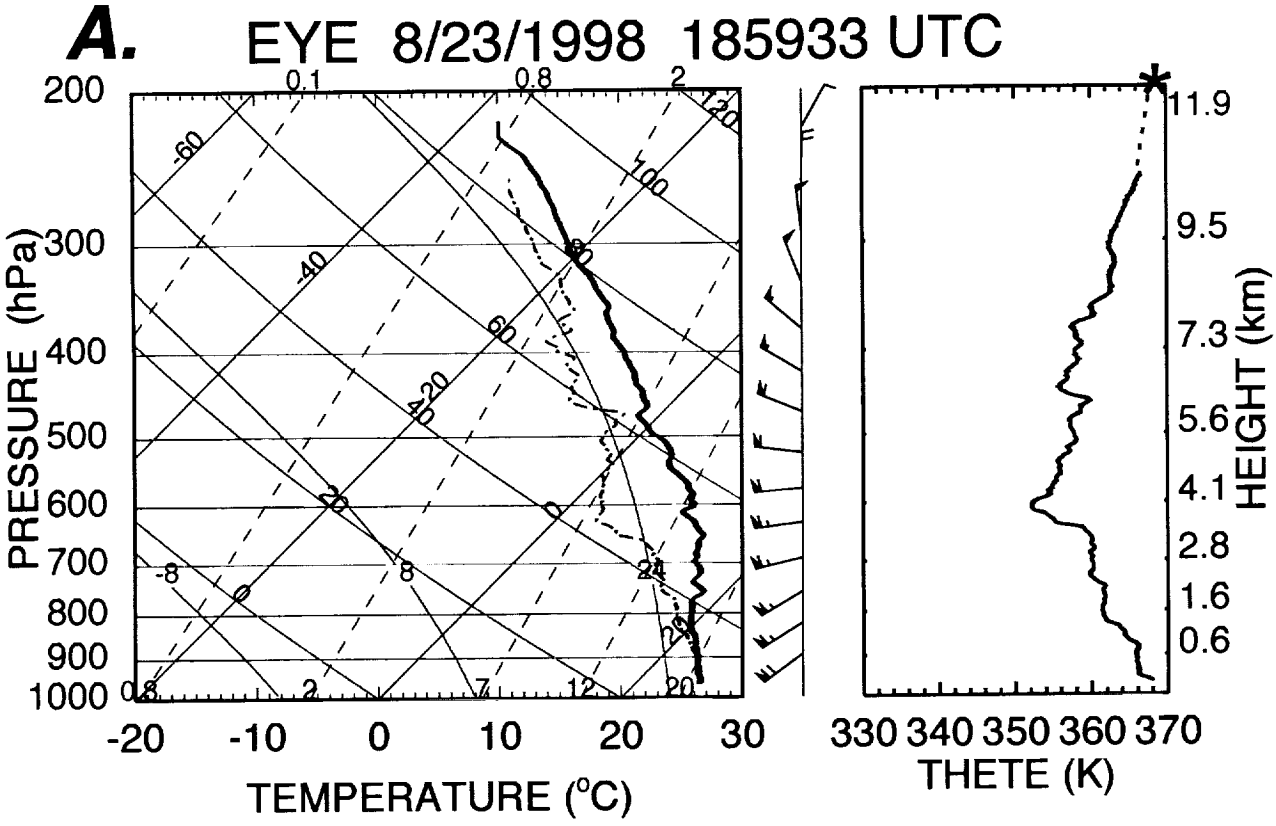
A.
EYE 8/23/1998 185933 UTC
PRESSURE (hPa)
TEMPERATURE (°C)
THETE (K)
HEIGHT (km)

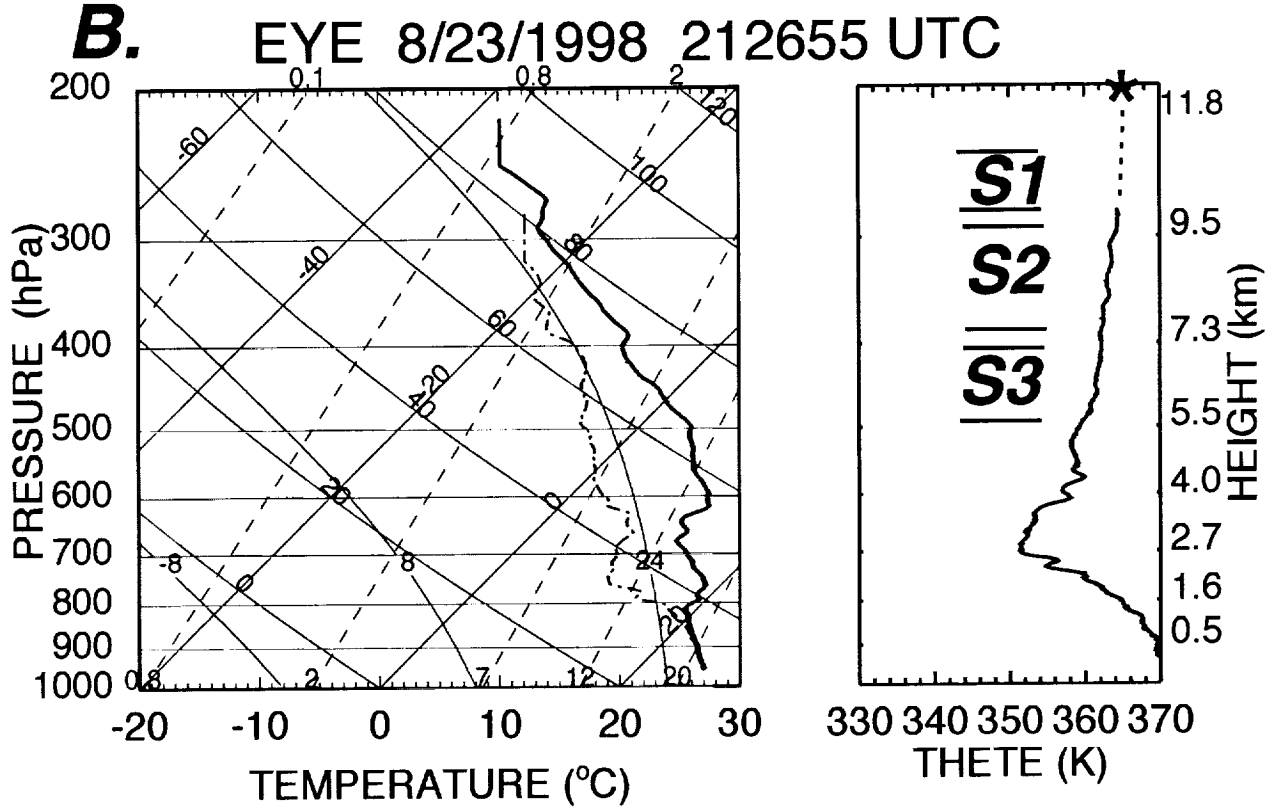
B.
EYE 8/23/1998 212655 UTC
S1
S2
S3
PRESSURE (hPa)
TEMPERATURE (°C)
THETE (K)
HEIGHT (km)

C. ENVIRONMENT 8/23/1998 194401 UTC

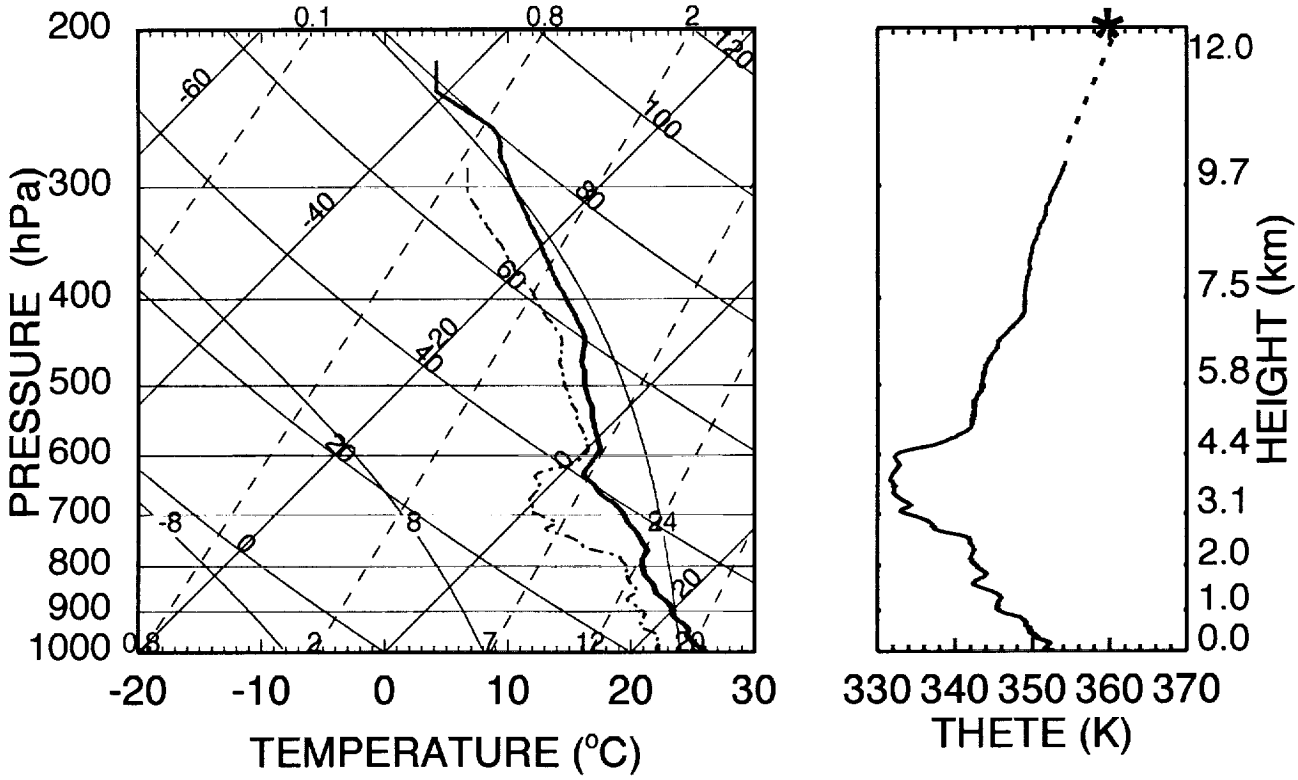

D. ENVIRONMENT 8/23/1998 204042 UTC

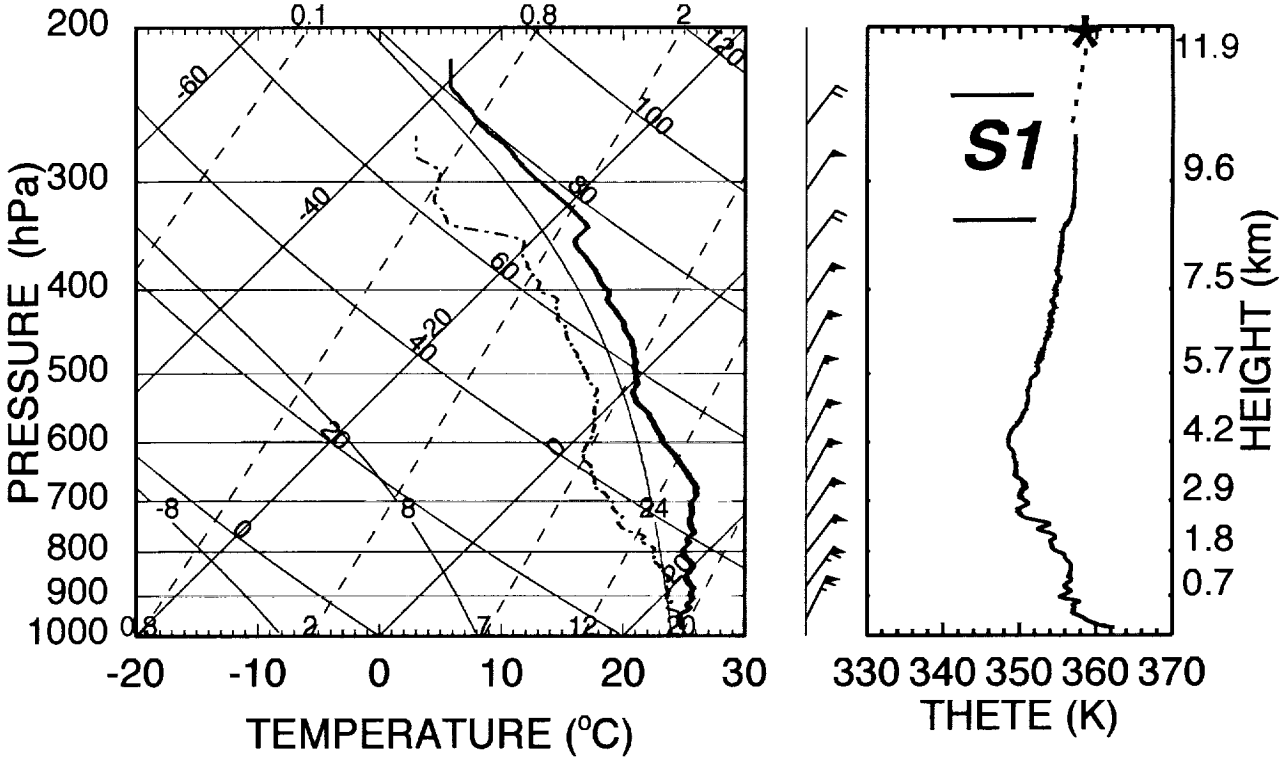

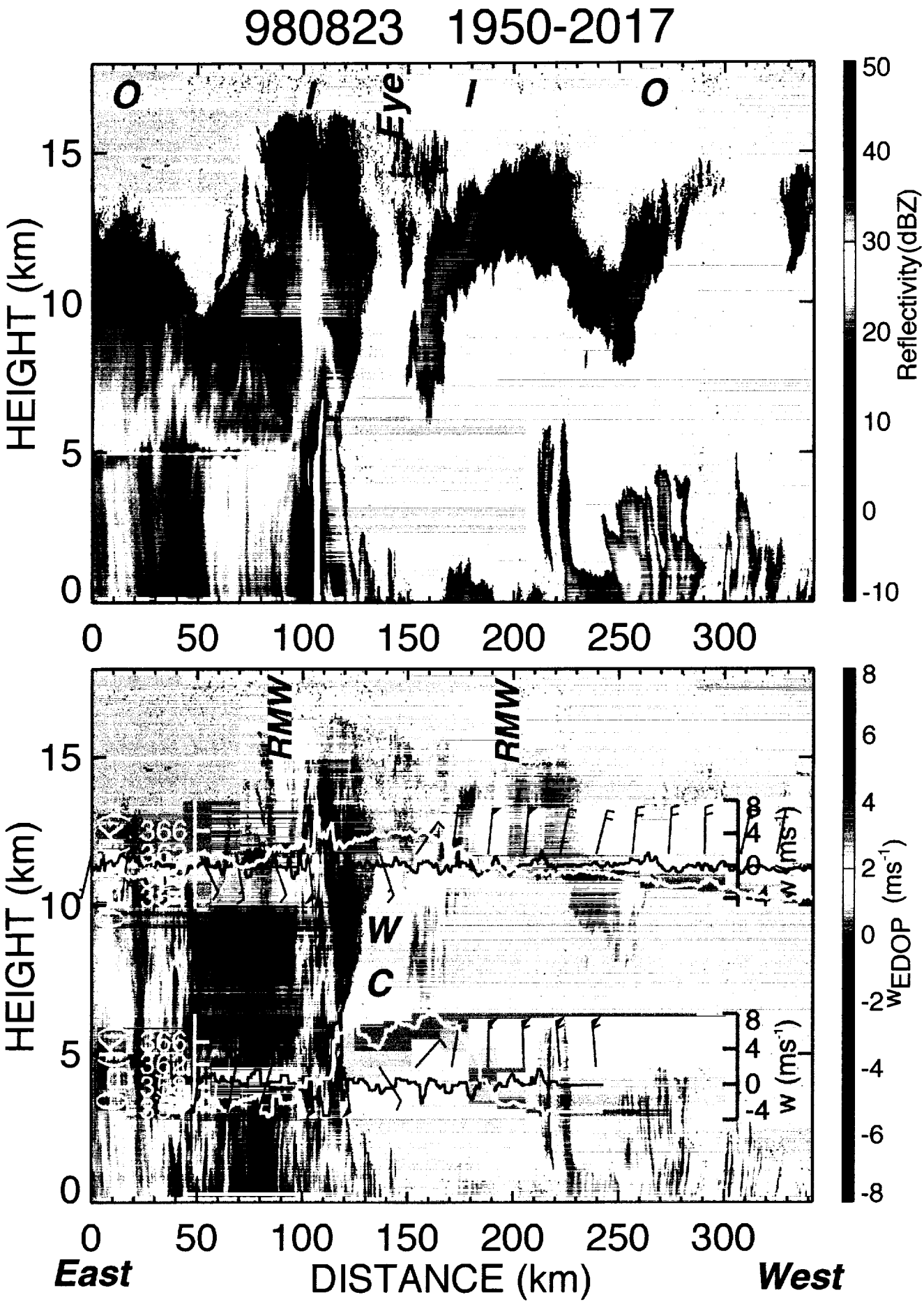
980823 1950-2017
O
I
Eye
I
O
HEIGHT (km)
15
10
5
0
0
50
100
150
200
250
300
Reflectivity(dBZ)
50
40
30
20
10
0
-10
RMW
RMW
W
C
366
w (ms-1)
8
4
0
-4
WEDOP (ms-1)
8
6
4
2
0
-2
-4
-6
-8
East
DISTANCE (km)
West

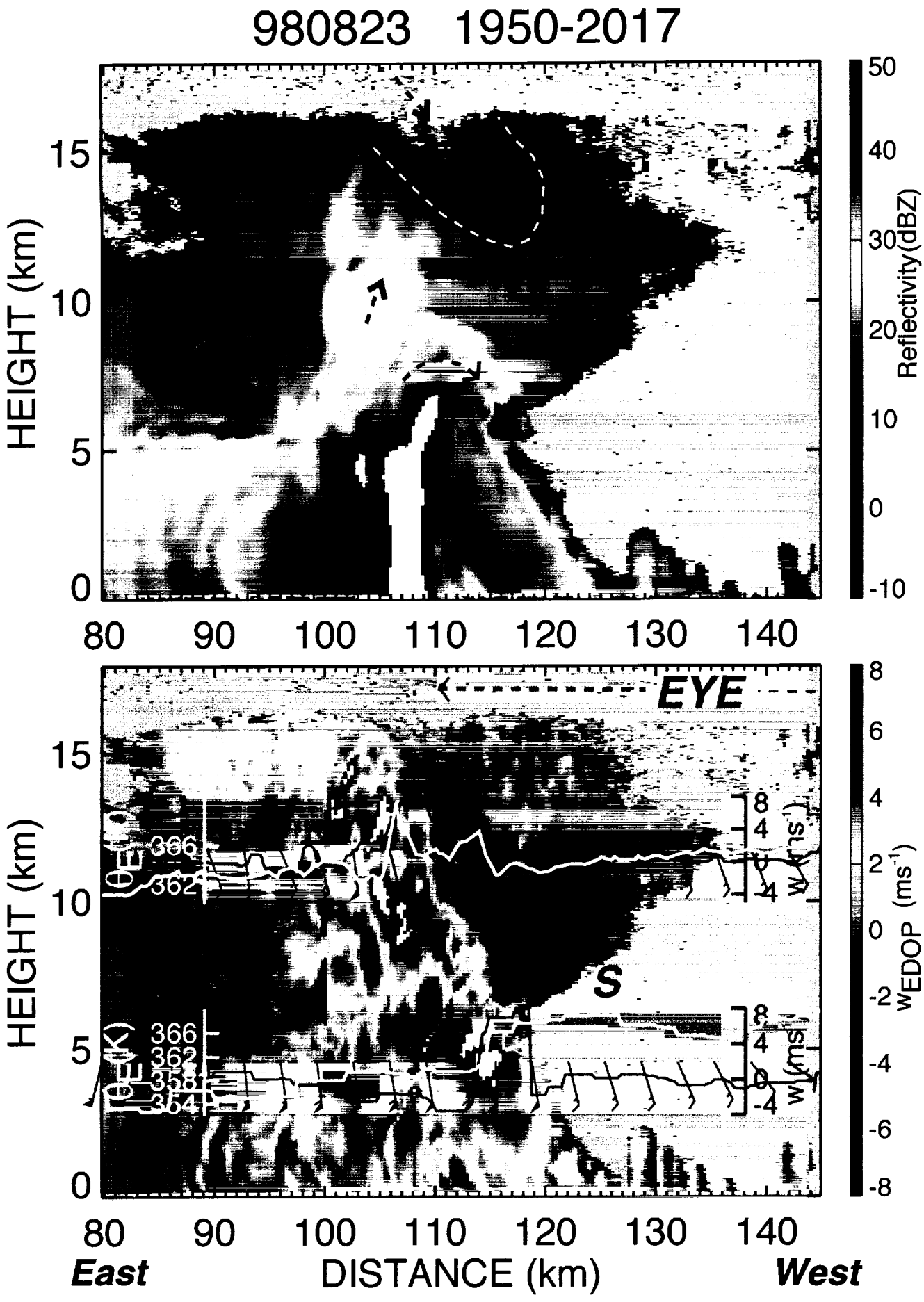
980823 1950-2017
HEIGHT (km)
15
10
5
0
80
90
100
110
120
130
140
50
40
30
20
10
0
-10
Reflectivity(dBZ)
EYE
S
θE (K)
366
362
358
354
8
4
0
-4
w (ms-1)
8
6
4
2
0
-2
-4
-6
-8
wEDOP (ms-1)
East
DISTANCE (km)
West

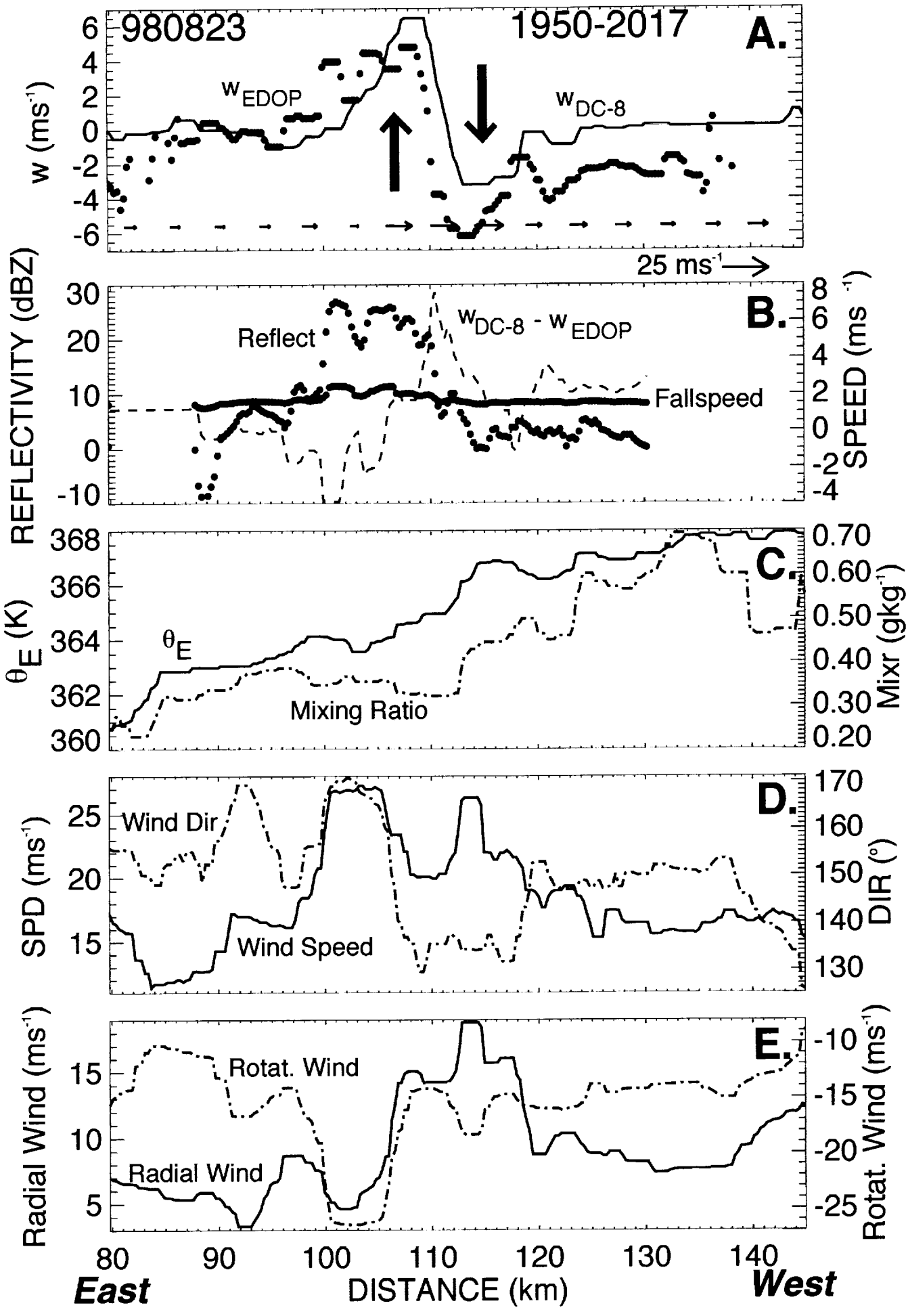
980823
1950-2017
A.
w (ms-1)
wEDOP
wDC-8
25 ms-1
B.
REFLECTIVITY (dBZ)
SPEED (ms-1)
Reflect
wDC-8 - wEDOP
Fallspeed
C.
θE (K)
Mixr (gkg-1)
θE
Mixing Ratio
D.
SPD (ms-1)
DIR (°)
Wind Dir
Wind Speed
E.
Radial Wind (ms-1)
Rotat. Wind (ms-1)
Rotat. Wind
Radial Wind
East
DISTANCE (km)
West

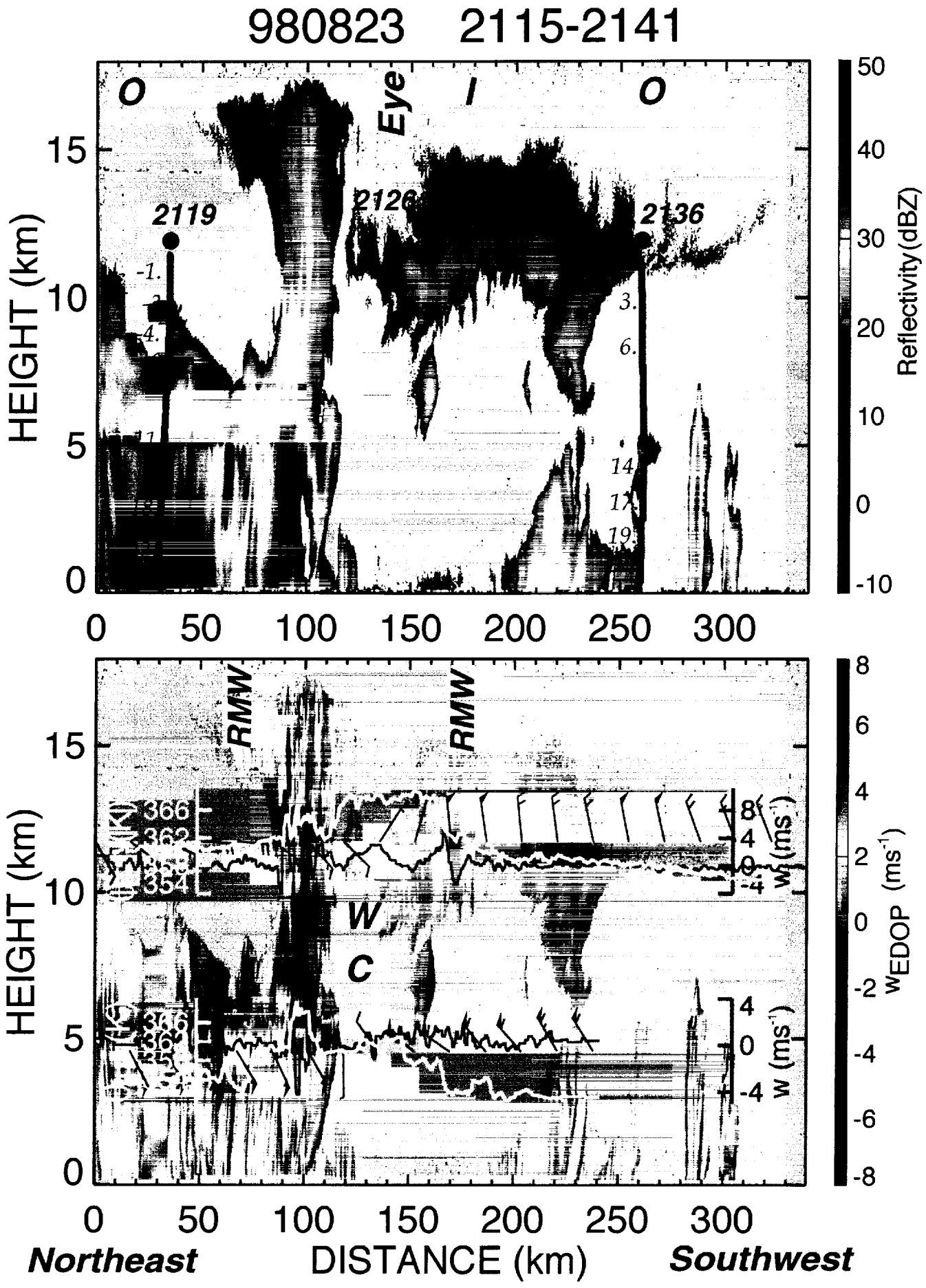
980823 2115-2141
O
Eye
I
O
2119
2126
2136
HEIGHT (km)
Reflectivity(dBZ)
RMW
RMW
W
C
w (ms-1)
wEDOP (ms-1)
Northeast
DISTANCE (km)
Southwest

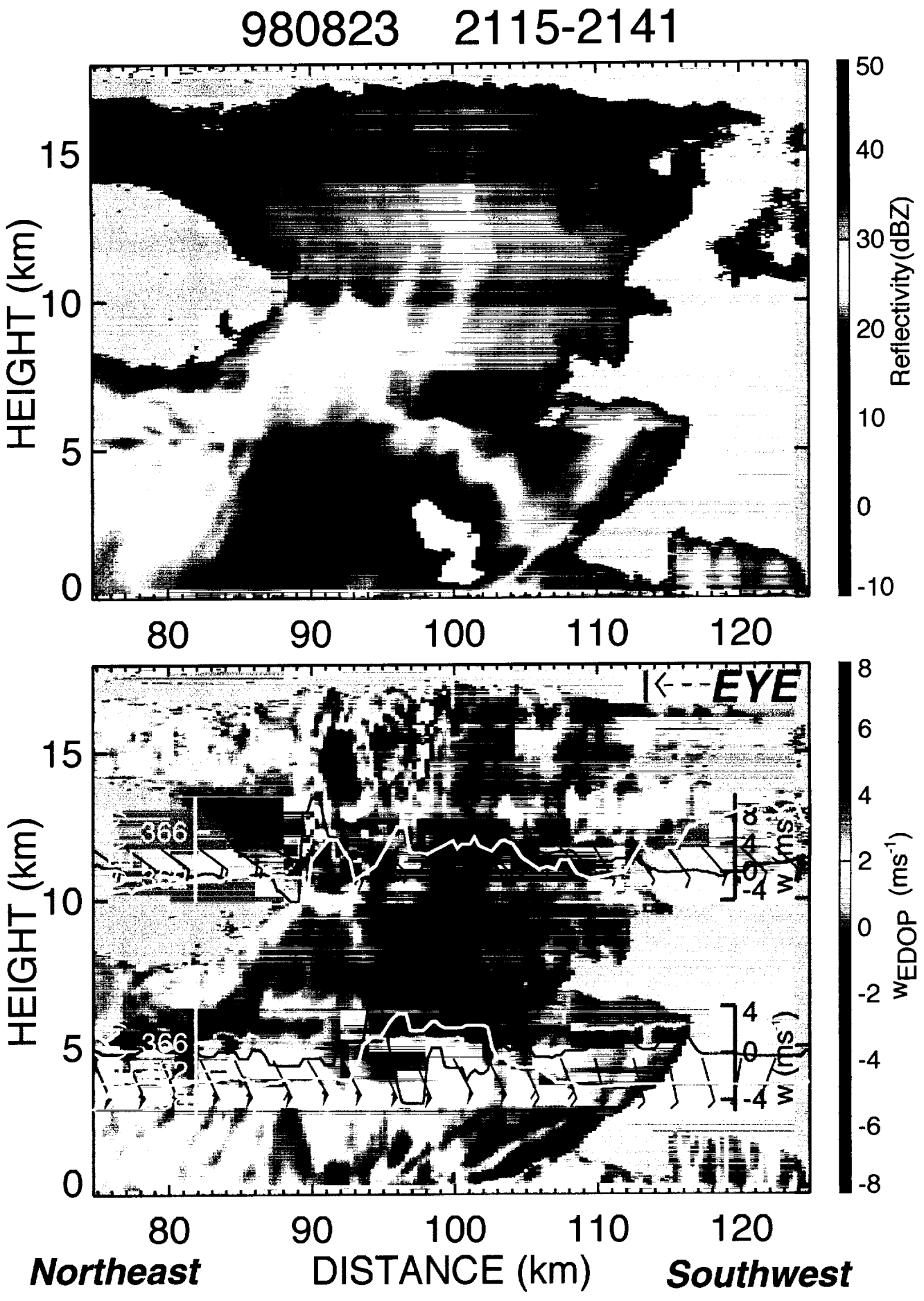
980823 2115-2141
HEIGHT (km)
15
10
5
0
80
90
100
110
120
50
40
30
20
10
0
-10
Reflectivity(dBZ)
EYE
366
366
α
4
0
-4
w (ms-1)
4
0
-4
w (ms-1)
8
6
4
2
0
-2
-4
-6
-8
wEDOP (ms-1)
Northeast
DISTANCE (km)
Southwest

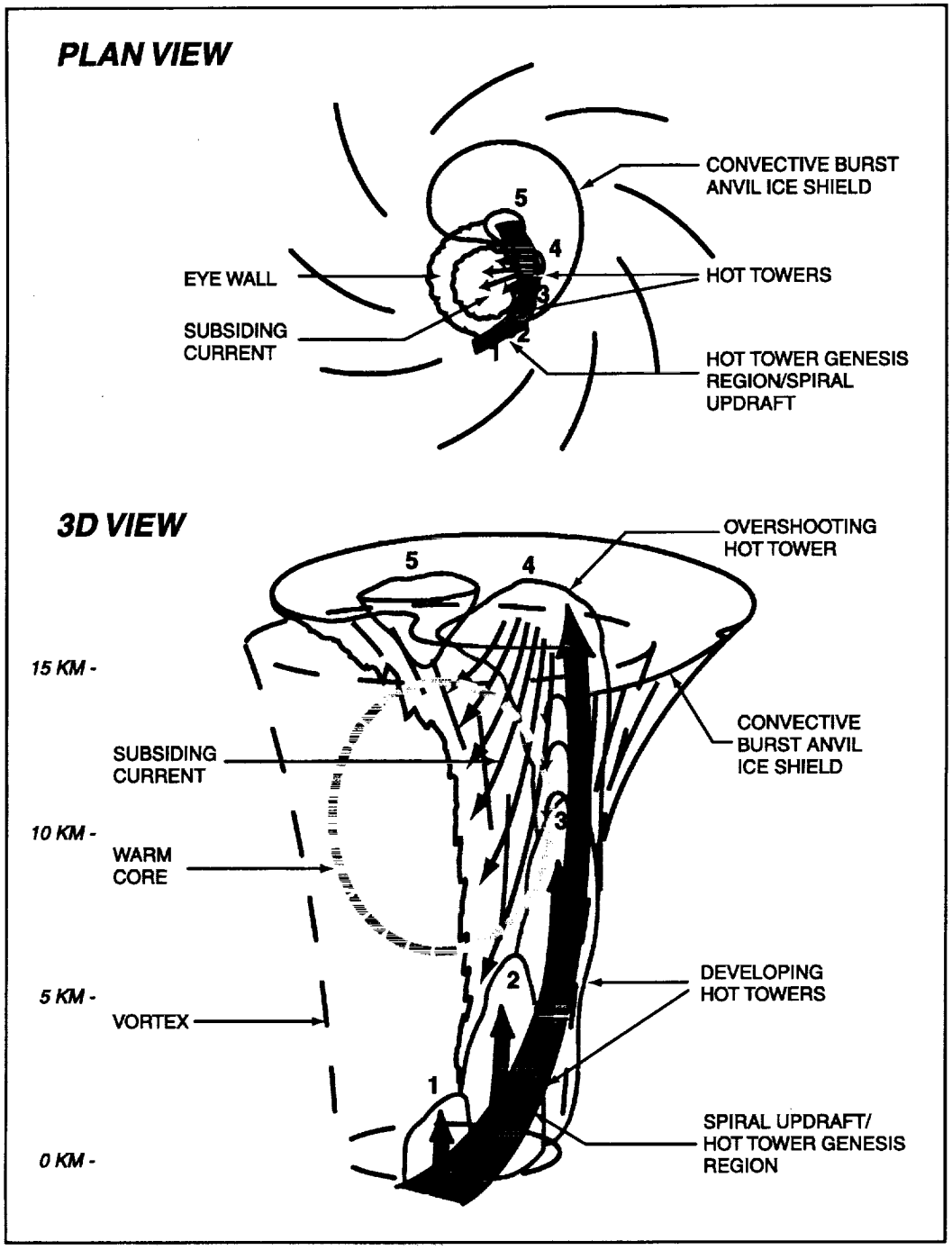
PLAN VIEW
CONVECTIVE BURST
ANVIL ICE SHIELD
5
4
EYE WALL
HOT TOWERS
3
SUBSIDING
CURRENT
2
HOT TOWER GENESIS
REGION/SPIRAL
UPDRAFT
3D VIEW
OVERSHOOTING
HOT TOWER
5
4
15 KM -
CONVECTIVE
BURST ANVIL
ICE SHIELD
SUBSIDING
CURRENT
10 KM -
3
WARM
CORE
DEVELOPING
HOT TOWERS
5 KM -
2
VORTEX
1
SPIRAL UPDRAFT/
HOT TOWER GENESIS
REGION
0 KM -